HHS Public Access

Author manuscript

Engineering (Beijing). Author manuscript; available in PMC 2025 May 06.

Published in final edited form as:

Engineering (Beijing). 2025 April ; 47: 130–138. doi:10.1016/j.eng.2024.11.030.

Acoustofluidics-Based Intracellular Nanoparticle Delivery

Zhishang Li[a,b,#], **Zhenhua Tian**[c,#], **Jason N. Belling**[d,e], **Joseph T. Rich**[b], **Haodong Zhu**[b], **Zhehan Ma**[b], **Hunter Bachman**[b], **Liang Shen**[b], **Yaosi Liang**[b], **Xiaolin Qi**[b], **Liv K. Heidenreich**[d,e], **Yao Gong**[d,e], **Shujie Yang**[b], **Wenfen Zhang**[f], **Peiran Zhang**[b], **Yingchun Fu**[a,*], **Yibin Ying**[a], **Steven J. Jonas**[d,g,h,i], **Yanbin Li**[j,*], **Paul S. Weiss**[d,e,k,l,*], **Tony J. Huang**[b,*]

[a]College of Biosystems Engineering and Food Science, Zhejiang University, Hangzhou 310058, China

[b]Department of Mechanical Engineering and Materials Science, Duke University, Durham, NC 27708, USA

[c]Department of Mechanical Engineering, Virginia Tech, Blacksburg, VA 24061, USA

[d]California NanoSystems Institute, University of California, Los Angeles, Los Angeles, CA 90095, USA

[e]Department of Chemistry and Biochemistry, University of California, Los Angeles, Los Angeles, CA 90095, USA

[f]College of Chemistry and Molecular Engineering, Zhengzhou University, Zhengzhou 450001, China

[g]Children's Discovery and Innovation Institute, University of California, Los Angeles, Los Angeles, CA 90095, USA

[h]Department of Pediatrics, David Geffen School of Medicine, University of California, Los Angeles, Los Angeles, CA 90095, USA

[i]Eli & Edythe Broad Center of Regenerative Medicine and Stem Cell Research, University of California, Los Angeles, Los Angeles, CA 90095, USA

[j]Department of Biological and Agricultural Engineering, University of Arkansas, Fayetteville, AR 72701, USA

[k]Department of Materials Science and Engineering, University of California, Los Angeles, Los Angeles, CA 90095, USA

[l]Department of Bioengineering, University of California, Los Angeles, Los Angeles, CA 90095, USA

[*]Corresponding authors. ycfu@zju.edu.cn (Y. Fu), yanbinli@uark.edu (Y. Li), psw@cnsi.ucla.edu (P.S. Weiss), tony.huang@duke.edu (T.J. Huang)..

[#]These authors contributed equally to this study.

Declaration of competing interest

Jason N. Belling, Liv K. Heidenreich, Steven J. Jonas, and Paul S. Weiss have patents related to this work. Zhishang Li, Zhenhua Tian, Joseph T. Rich, Haodong Zhu, Zhehan Ma, Hunter Bachman, Liang Shen, Yaosi Liang, Xiaolin Qi, Yao Gong, Shujie Yang, Wenfen Zhang, Peiran Zhang, Yingchun Fu, Yibin Ying, Yanbin Li, and Tony J. Huang declare that they have no known competing financial interests or personal relationships that could have appeared to influence the work reported in this paper.

Abstract

Controlled intracellular delivery of biomolecular cargo is critical for developing targeted therapeutics and cell reprogramming. Conventional delivery approaches (e.g., endocytosis of nano-vectors, microinjection, and electroporation) usually require time-consuming uptake processes, labor-intensive operations, and/or costly specialized equipment. Here, we present an acoustofluidics-based intracellular delivery approach capable of effectively delivering various functional nanomaterials to multiple cell types (e.g., adherent and suspension cancer cells). By tuning the standing acoustic waves in a glass capillary, our approach can push cells in flow to the capillary wall and enhance membrane permeability by increasing membrane stress to deform cells via acoustic radiation forces. Moreover, by coating the capillary with cargo-encapsulated nanoparticles, our approach can achieve controllable cell-nanoparticle contact and facilitate nanomaterial delivery beyond Brownian movement. Based on these mechanisms, we have successfully delivered nanoparticles loaded with small molecules or protein-based cargo to U937 and HeLa cells. Our results demonstrate enhanced delivery efficiency compared to attempts made without the use of acoustofluidics. Moreover, compared to conventional sonoporation methods, our approach does not require special contrast agents with microbubbles. This acoustofluidics-based approach creates exciting opportunities to achieve controllable intracellular delivery of various biomolecular cargoes to diverse cell types for potential therapeutic applications and biophysical studies.

Keywords

Acoustofluidics; Sonoporation; Nanocarriers; Metal-organic frameworks

1. Introduction

The effective intracellular delivery of biomolecular cargos is critical across several biomedical research areas, including gene therapies, cell reprogramming, vaccine development, drug delivery, and nanomedicine. Engineering solutions that facilitate transport of therapeutics and/or genetic engineering reagents into cells play a crucial role in advancing our understanding of cellular processes and developing therapeutic interventions [1,2]. To deliver a desired cargo to a target cell successfully, it must cross the cell's semi-permeable outer lipid membrane. To date, various approaches have been developed, including passive approaches based on viral [3] or non-viral vectors [4] that can facilitate the uptake process, as well as active approaches that are able to open micropores along cell membranes (e.g., sonoporation [5], electroporation [6], mechanical membrane disruption [7–9], thermal membrane disruption [10,11], and microinjection [12]).

Among the vector-based methods [13], various viral vectors are widely used in clinical and translational studies because of their efficiencies and specificities [14]. However, clinical-grade viral vectors are limited by their high manufacturing costs, complex processing requirements, potential insertional genotoxicity and immunogenicity, and relatively low packaging capacities [15]. Given these drawbacks, non-viral vectors such as polymer [16–18], inorganic material [19], lipid [20], and exosome-based nanocarriers [21,22] offer attractive alternatives. Different cargo types (e.g., therapeutic molecules, gene-editing tools,

reprogramming factors, and proteins) can be loaded into nanocarriers and then delivered to target cells [23]. Once the nanocarriers enter a cell, additional stimuli are often used to trigger the cargo release process [24]. Even though there have been significant advances in the development of different nanocarriers to enhance the delivery efficiency [25–28], multiple challenges remain to be addressed. These obstacles include nanocarrier aggregation [29], slow uptake of cargo entering the cytoplasm, high ratios of residual nanocarriers (i.e., those left in the extracellular medium), and a lack of efficient and controllable mechanisms that facilitate cell-nanocarrier contact, membrane-nanocarrier bonding, and ultimately nanocarrier transport across the cellular membranes [30].

Vector-free approaches, which can actively facilitate the formation of pores at cellular membranes for the diffusion of cargo into cells have attracted great interest [23]. However, these approaches are often limited by low recovery rates, dependence on certain cell types, and/or costly equipment [31]. These technologies are also susceptible to damaging critical cellular components, lowering cell viability, and/or reducing the effectiveness/functionality of the cargo delivered [32]. For example, conventional microbubble-based sonoporation approaches usually require specific contrast agents contained within microbubbles [5], which can cause irreparable damage to targeted cells, lowering their viability (e.g., to below 50% in some studies) [33,34].

The convergence of acoustic waves and microfluidics (i.e., acoustofluidics) offers a powerful tool for active nanomaterial manipulation and delivery [22,35–50]. Several groups have explored the development of various bubble-free sonoporation approaches [51] to address issues associated with microbubble contrast agents, which leverage focused acoustic waves [33], surface acoustic waves [52,53], spiraling acoustical tweezers [54], or hyperfrequency acoustic streaming [55]. The throughputs of these approaches are still low because they are limited to the sonoporation of cells in a small area targeted by focused acoustic waves, in small microfluidic chambers, or in regions near the hyperfrequency acoustic source. To increase sonoporation throughput, we have recently developed a platform based on the application of standing bulk acoustic waves in a capillary that achieved high-throughput delivery of expression plasmid to human hematopoietic stem cells and other primary cell types [56]. The motivation was to overcome the channel clogging by cell debris limiting prior methods of cell deformation in physical constrictions in microfluidic channels [56,57]. Previous sonoporation approaches induce the opening of membrane pores [23,58,59], but the cargo nevertheless relies on diffusion-based transport for entry into cells. This diffusion-based mechanism relies on high concentrations of cargo in the extracellular medium. It also leads to low cargo usage rates (i.e., ratios between cargos delivered to cells and cargos left in the extracellular medium), which is a critical factor that must be considered when delivering expensive cargos.

In this study, we present an acoustofluidics-based intracellular delivery approach that can be used to deliver functional cargos encapsulated in metal organic framework-based nanoparticles efficiently and biocompatibly to immortalized cancer cell lines (e.g., U937 and HeLa). Our approach leverages standing acoustic waves generated in a glass capillary coated with cargo-encapsulated nanoparticles. By tuning the acoustic wave frequency to align the generated acoustic pressure node line along the capillary wall, our approach can push cells

in flow to the nanoparticle-coated capillary wall using acoustic radiation forces, achieving controllable cell-nanoparticle contact and facilitating membrane-nanoparticle attachment. This feature decreases the random nature of cell-nanoparticle interactions through Brownian movement that limits conventional nanocarrier-based delivery approaches [55,60]. Our approach facilitates nanoparticle uptake by pressing the cells onto the nanoparticle coated capillary as well as increasing the membrane stress via acoustic radiation forces. Additionally, our approach does not need the bubbles or special acoustic contrast agents that are usually required in conventional sonoporation methods.

To investigate the mechanism of our approach and to characterize its performance, we performed finite element simulations and a series of experiments to deliver different types of cargo to U937 and HeLa cancer cell lines. The nanocarriers used in this research are based on zeolitic imidazolate framework-8 (ZIF-8) nanoparticles, that is, porous nanomaterials that can be loaded with different biomolecular cargos such as camptothecin, doxorubicin (DOX) [61], DNA [62], and clustered regularly interspaced short palindromic repeats (CRISPR)/Cas9 [63]. Two types of cargo were used in this work, DOX and fluorescein isothiocyanate (FITC)-labeled bovine serum albumin (FBSA), to investigate the delivery of small-molecule and protein-based cargos. Both simulations and experimental results show that our acoustofluidic approach enables active cell-nanoparticle contact to facilitate cell-nanoparticle attachment as well as increases the membrane permeability to assist in nanoparticle uptake. Moreover, different cargos can be successfully delivered into the cells with enhanced efficiency. Altogether, this contrast agent-free, acoustofluidic method informs future intracellular delivery technologies that are biocompatible, efficient, and controllable for therapeutic applications and biophysical studies.

2. Experiments

2.1. Synthesis of cargo-loaded ZIF-8 nanoparticles

Preparation of DOX-loaded ZIF-8 (denoted as DOX@ZIF-8) nanoparticles was conducted following procedures reported previously [50]. Different loading rates can be achieved by using different DOX concentrations during synthesis. We used 1 mL of 6 mg•mL^{-1} DOX in the experiments. The solutions were mixed with 200 μL of 0.8 mol•L^{-1} $Zn(NO_3)_2$ (pH adjusted to 8.0 using NaOH) and agitated vigorously for 10 min, followed by a dropwise addition of 2 mL of 3 mol•L^{-1} 2-methylimidazole solution. After 15 min, the DOX encapsulated nanoparticles were collected following three cycles of centrifugation at 8000 r•min^{-1}, washed with water, and dried at 60 °C overnight. For the preparation of FBSA-loaded ZIF-8 (denoted as FBSA@ZIF-8) nanoparticles, 100 μL of 2 mg•mL^{-1} FBSA was added into 2 mL of 3 mol•L^{-1} 2-methylimidazole solution and stirred for 30 min. Then, 200 μL of 0.4 mol•L^{-1} $Zn(NO_3)_2$ was added to the mixture and magnetically stirred for 15 min. The yellow solution was centrifuged at 8000 r•min^{-1} and washed with deionized (DI) water three times, followed by drying at 65 °C overnight.

2.2. Device fabrication

The acoustofluidics-based intracellular delivery device was composed of a lead zirconate titanate (PZT) plate-type transducer (Steminc-Piezo, USA) and a square capillary

(VitroCom, USA). The transducer was fixed onto a glass slide (VWR, USA) using two pieces of double-sided adhesive tape attached to polyurethane spacers (thickness: 2 mm). Then, the capillary was bonded to the top of the transducer using epoxy (Permatex, USA). To generate standing acoustic waves, it is important to consider the acoustic frequency and the size of the glass capillary [64]. A transducer with a resonant frequency of 710–720 kHz was used to generate standing bulk acoustsic waves in a 200 μm × 200 μm × 50 mm glass capillary. At this frequency, our device can generate a pressure node line along the capillary wall. Two tubes were connected to the end of the glass capillary. To coat the synthesized nanoparticles (e.g., ZIF-8, DOX@ZIF-8, and FBSA@ZIF-8) onto glass capillaries, nanoparticle solutions were injected into the glass capillaries, which were then placed horizontally in an oven. After drying each capillary at 65 °C overnight, a layer of nanoparticles remained on the bottom wall of the capillary.

2.3. Device operation

The fabricated device was mounted to an inverted microscope (Nikon, Japan). Cells were loaded into a 1 mL syringe (BD Biosciences, USA) and pumped into the glass capillary at a flow rate controlled by an automatic syringe pump (neMESYS, Cetoni, Germany). The excitation signal for the piezoelectric transducer was generated using a function generator (Agilent, USA) and then amplified with a power amplifier (Amplifier Research, USA). During the delivery experiments, a fan was used to cool the acoustofluidic device.

2.4. Release of FBSA and DOX from ZIF-8 nanoparticles

To evaluate the release of cargo from the cargo-encapsulated ZIF-8 nanoparticles, 2 mg of nanoparticles were dispersed in 10 mL of phosphate-buffered saline (PBS) at either pH 5.0 or 7.2. At different time points (1, 3.5, 4.5, 5.5, 15.5, 18.5, 36, 72, 96, 120, 140, 160, 180, and 240 h), 1 mL was taken from the solution and centrifuged at 6000 r•min^{-1}. For each measurement, 200 μL of the supernatant was added into a 96-well plate and measured with a microplate reader. After each measurement, the sample was returned to the bulk solution for future analysis.

2.5. Cell culture and viability assay

U937 and HeLa cells were purchased from ATCC (Virginia, USA). U937 and HeLa cells were cultured in Roswell Park Memorial Institute-1640 medium (Thermo Fisher Scientific, USA) and Dulbecco's Modified Eagle Medium (Thermo Fisher Scientific, USA), respectively, supplemented with 10% (v/v) fetal bovine serum. The medium was exchanged every two days. To evaluate cell viability, cells were stained with Calcein acetoxymethyl ester (C3100MP, Life Technologies, USA), and those exhibiting green fluorescence were counted as live cells. Cell viability was determined by the ratio of live cells to the total number of cells.

2.6. Delivery efficiency

The delivery efficiency was determined by counting the numbers of fluorescent cells in acquired microscopy images. The cell intensity was calculated using ImageJ (National institutes of Health, USA). Flow cytometry (BD FACSCanto II, USA) was used for the

quantitative evaluation of the nanoparticle delivery efficiency. The collected cells were washed and redispersed in PBS before flow cytometry. For each characterization group, three samples were tested to calculate the standard deviation. The data were analyzed using FlowJo (BD Biosciences, USA).

3. Results and discussion

3.1. Mechanism and design of the acoustofluidics-based intracellular delivery device

Fig. 1(a) shows a schematic of our acoustofluidics-based intracellular delivery device, which is composed of a square glass capillary coated with cargo-encapsulated nanoparticles and a piezoelectric transducer to generate incident acoustic waves. Details of the device fabrication can be found in the Section 2. Notably, the capillary's inner dimension is smaller than a quarter wavelength of the acoustic waves generated from the transducer. This geometric constraint enables the generation of a pressure node line along the capillary's inner wall (see Fig. 1(b) for a cross-sectional illustration). As cells are flowed through the capillary coated with cargo-encapsulated nanoparticles (Fig. 1(c)), the acoustic radiation force moves the cells to the pressure node line and pushes them against the capillary wall, where the cells can directly contact the coated nanoparticles. This controllable cell-nanoparticle interaction can facilitate nanoparticle transfer and attachment on the cell's membrane. Moreover, the acoustic radiation force applied on the membrane and the reaction force applied through the cell membrane-capillary wall interaction can increase membrane stress and slightly deform the cells. These forces facilitate nanoparticle entry across the cell membrane. Based on these capabilities, our acoustofluidics-based intracellular delivery device enables controlled delivery of cargo-encapsulated nanoparticles to cells.

In this study, ZIF-8 nanoparticles were used as the nanocarriers because of their ability to encapsulate various molecular cargos and deliver them into cells through endocytosis [61,65]. Fig. 1(d) provides a flow diagram detailing the steps for delivering cargo-encapsulated ZIF-8 nanoparticles and releasing the cargo. Cells that are flowed through our device with acoustic waves on are pushed to the glass capillary wall, enabling cell-nanoparticle contact. This process facilitates the cell-nanoparticle bonding and the intracellular entry of the nanoparticles via endocytosis. When the cargo-encapsulated ZIF-8 nanoparticles are delivered to the cytoplasm within endosomes, cargo is released by endosomal escape as the ZIF-8 nanocarriers gradually break down in this acidic environment [63,66]. Note that no acoustic waves are applied to cells during the cargo release process. Whether acoustic waves can facilitate the cargo release is an interesting question that will be explored in future studies.

3.2. Capillaries coated with cargo-encapsulated ZIF-8 nanoparticles

We performed a series of experiments to characterize the properties of the cargo-encapsulated ZIF-8 nanoparticles used in this study and better understand the cargo encapsulation and release processes. Two types of cargos (i.e., DOX and FBSA) were used to investigate our device's ability to deliver small molecule and protein-based cargos [61,67]. By following the procedures summarized in the Section 2, we synthesized DOX@ZIF-8 and FBSA@ZIF-8 nanoparticles and then characterized the synthesized

nanoparticles using multiple techniques, including transmission electron microscopy (TEM), dynamic light scattering (DLS), powder X-ray diffraction (PXRD), and ultraviolet-visible (UV-Vis) spectroscopy (Fig. 2).

From the TEM images (Figs. 2(a) and (b)), we found that the diameters of DOX@ZIF-8 and FBSA@ZIF-8 nanoparticles were approximately 150 nm. The size distributions measured by number-weighted DLS measurements (Fig. 2(c)) indicated that 60%, 83%, and 82% of the particles were in the 100–250 nm range for ZIF-8, DOX@ZIF-8, and FBSA@ZIF-8, respectively. The cargo-loaded ZIF-8 nanoparticles exhibited a more polydisperse size distribution compared to ZIF-8. This could be due to aggregation of the amorphous precursors induced by FBSA and DOX encapsulation during the ZIF-8 nucleation stage [67]. The PXRD distributions (Fig. 2(d)) for ZIF-8, DOX@ZIF-8, and FBSA@ZIF-8 nanoparticles show similar trends, indicating that these nanoparticles have similar crystalline structures. The packaging of cargo into the ZIF-8 nanocarriers was characterized using UV-Vis spectroscopy. The FBSA@ZIF-8 nanoparticles (Fig. 2(e)) exhibit an absorbance peak at 500 nm, indicating the successful encapsulation of FBSA proteins [67]. The DOX@ZIF-8 nanoparticles (Fig. 2(f)) have an absorbance peak at 490 nm, indicating successful loading of DOX molecules [68]. The pH-dependent cargo release was investigated by dissolving cargo-encapsulated nanoparticles in solutions with different pH values and measuring the absorbance spectrum change through UV-Vis spectroscopy. The result (Fig. S1 in Appendix A) shows that cargo can remain in the ZIF-8 nanoparticles in a non-acidic (pH 7.4) environment for at least 10 days. In contrast, the ZIF-8 nanoparticles gradually decompose in an acidic (pH 5.0) environment.

Next, the prepared DOX@ZIF-8 and FBSA@ZIF-8 nanoparticles were coated on the inner walls of the glass capillaries (Section 2). The uncoated capillaries presented a smooth wall (Fig. 2(g)) and no fluorescence within the channel (Fig. 2(j)). Bright-field and fluorescence microscopy was used to confirm successful coating of DOX@ZIF-8 (Figs. 2(h) and (k)) and FBSA@ZIF-8 (Figs. 2(i) and (l)) nanoparticles onto the capillary wall, respectively. The capillaries coated with ZIF-8 nanoparticles were subsequently used for intracellular delivery experiments.

3.3. Acoustofluidics-enabled cell movement, deformation, and permeability change

To investigate our device's capabilities, such as acoustic wave-induced cell movement, deformation, and permeability change, we performed both finite element simulations and cell tracking experiments. The finite element simulations were performed in COMSOL Multiphysics 5.4 (Stockholm, Sweden) at an excitation frequency of 710 kHz and an amplitude of 20–25 Vpp (matching the experimental parameters, Vpp: voltage-peak to peak). The simulation results are given in Figs. 3(a)–(d). The displacement field (Fig. 3(a)) shows a resonant mode at the excitation frequency with dominated z-direction displacements. The standing acoustic pressure field in the fluid domain (Fig. 3(b)) shows a low-pressure region near the top boundary. The simulated acoustic radiation force (Fig. 3(c)) shows a strong $+z$ component. Therefore, cells randomly distributed in the capillary can be moved to the top wall, as illustrated by the cell movement trajectories induced by the acoustic waves (Fig. 3(d) and Movie S1 in Appendix A). To validate the cell movement

predicted by finite element simulations, experiments were performed by loading cells into a capillary and monitoring cell movement induced by acoustic waves through a microscope. The captured images (Figs. 3(e)–(g)) show that randomly distributed cells in a capillary can be moved rapidly to the capillary's top wall when acoustic waves are generated. Fig. 3(f) reveals the cell trajectories by stacking together multiple frames of a recorded video. This experimentally acquired cell trajectory is consistent with the simulation result in Fig. 3(d). In addition to the case without flowing cell culture medium through the system, we performed similar experiments where cell solutions were passed through capillaries at a flow rate of 5 $\mu L \cdot min^{-1}$. Movies S2 in Appendix A show our device can push flowing cells to the capillary wall using acoustic waves.

To investigate our device's capability to increase membrane permeability, we loaded a solution containing both U937 cells and DOX@ZIF-8 nanoparticles into two uncoated capillaries (one with acoustic waves off and one with the acoustic waves on). The tested cells were collected, washed, and imaged using fluorescence microscopy. In the control group, where acoustic waves were absent, the observed fluorescence intensities of the cells (Fig. 3(h)) were notably weak. Conversely, in the group exposed to active acoustic waves, the cells exhibited higher fluorescence intensities from DOX (Fig. 3(i)), suggesting markedly enhanced uptake of DOX@ZIF-8 nanoparticles. These results indicate that our acoustofluidic device increases nanoparticle uptake. The observed enhancement in nanoparticle internalization could be related to the increased lipid membrane stress and slight cell deformation observed during acoustofluidic treatment (Fig. S2 in Appendix A) [58,69], which are induced by the acoustic radiation force directly applied to the cells, the reaction force from cell–cell interactions, and the reaction force from the cell-capillary wall interaction.

As indicated by the numerical and experimental results, our acoustofluidic device is capable of overcoming Brownian movement between nanoparticles and target cells to facilitate cell-nanoparticle attachment and changing membrane permeability. The combination of these capabilities enables effective intracellular transport of the nanoparticles. Next, we explored whether our acoustofluidic device could be used for delivering ZIF-8 nanoparticles loaded with different cargos (i.e., FBSA and DOX) into various types of cells (i.e., U937 and HeLa cells).

3.4. Delivery of cargo-encapsulated ZIF-8 nanoparticles to different types of cells

We performed additional experiments to demonstrate the delivery of cargo-encapsulated ZIF-8 nanoparticles using our acoustofluidics-based approach. To investigate the delivery of ZIF-8 nanoparticles loaded with different cargos (e.g., FBSA and DOX), experiments were performed by running two groups of U937 cells (concentration: 2×10^6 cells mL^{-1}, flow rate: 5 $\mu L \cdot min^{-1}$) through acoustofluidic devices, one with FBSA@ZIF-8 and one with DOX@ZIF-8 coatings. The collected cells were washed three times with PBS, seeded in a Petri dish, cultured for 30 min, and then imaged with a fluorescence microscope (TE2000-U, Nikon, Japan). The acquired microscopy images are shown in Figs. 4(a)–(d). The control groups without acoustic waves show low fluorescence intensities (Figs. 4(a) and (c)). In contrast, higher fluorescence intensities are observed for cell populations exposed to

acoustic waves (green in Fig. 4(b) and red in Fig. 4(d)), indicating higher nanoparticle delivery yields. To characterize the intensity differences between groups with acoustic waves on and off, the mean fluorescence intensity for cells in each group was calculated using ImageJ (Fig. S3 in Appendix A). By comparing these results for the delivery of DOX@ZIF-8 nanoparticles, the mean fluorescence intensity for the acoustics-on group was at least twice that of the acoustics-off group. The delivery of FBSA@ZIF-8 nanoparticles by the acoustic waves shows greater intensity enhancement.

To investigate the effects of nanocarrier (ZIF-8 only) decomposition and acoustic waves on cell viability, calcium AM-based cell viability assays (detailed procedures in Section 2) were performed on U937 cells treated under three different conditions: ① acoustics off without ZIF-8 coating, ② acoustics on without ZIF-8 coating, and ③ acoustics on with ZIF-8 coating. The results are presented in Fig. 4(e). Comparing the results of conditions ① and ②, we found a slight decline in cell viability, from 93% to 85%, when acoustic waves were applied in devices without ZIF-8 nanocarriers. Comparing the results of conditions ② and ③, we observed that cell viability at 24 h decreased slightly from 85% to 78%. After the 24 h period, the viability for the ZIF-8 coating group is about 80%. These results indicate that the ZIF-8 nanocarrier decomposition and the used acoustic waves have minimal effects on cell viability.

To determine whether our acoustofluidic device can deliver cargo-encapsulated ZIF-8 nanoparticles into cells and whether the cargo released into the cells remained functional, we performed experiments using U937 cells under different delivery conditions (i.e., acoustics off/on with DOX@ZIF-8 coating). The cargo used in these experiments is DOX, a common chemotherapeutic agent that can cause cell apoptosis [70]. We examined the DOX-related cytotoxicity resulting from our nanoparticle delivery by characterizing cell viability at 0.5, 2, 8, and 24 h after flowing U937 cells through our acoustofluidic device. The collected cells were washed with PBS and cultured prior to performing calcium AM-based viability assays. The results in Fig. 4(f) show that cell viability for the group without acoustic waves is about 90% in 0.5 to 24 h. However, for the group treated with acoustic waves, the cell viability at 24 h declines to 53%, demonstrating the effectiveness of acoustofluidics-facilitated delivery. The comparison between groups with and without acoustic waves indicates that the DOX@ZIF-8 nanoparticles have been delivered into cells, releasing the DOX cargo. Moreover, the DOX cargo released into cells remains functional [61].

Additional experiments of the DOX@ZIF-8 delivery and DOX release processes were performed. HeLa cells suspended in PBS were treated using acoustofluidic devices coated with DOX@ZIF-8 nanoparticles. To determine how cells interact with the coated nanoparticles on the capillary walls, we recorded a video of HeLa cells flowing through a capillary (cell concentration: 2×10^6 cells mL^{-1}, flow rate: 5 μL min^{-1}). Our results (Fig. 5(a) and Movie S3 in Appendix A) show that the acoustic waves generated by a PZT transducer installed at the bottom side of the capillary can force cells to move through the capillary along the top wall. We observed that the original nanoparticle coating (~5 μm thick) becomes thinner (Fig. 5(b)), after running 1 mL of the cell solution through our device. This observation results from nanoparticles coated on the capillary wall being transferred to the membranes of the targeted cells, as shown in a bright-field

microscopy image acquired at 5 min after the experiment (Fig. 5(c)). These experimental observations confirm that our acoustofluidic device can facilitate cell-nanoparticle contact. To investigate the release of cargo from DOX@ZIF-8 nanoparticles, the collected HeLa cells were washed with PBS, cultured for 6 h, stained, and then imaged via fluorescence microscopy. The acquired fluorescence images show that DOX (red) was well distributed in the cytoplasm (Fig. 5(d)). The observed DOX cargo was released from the successfully delivered DOX@ZIF-8 nanoparticles via an endosomal escape process whereby the ZIF-8 framework begins to decompose when exposed to the acidic environment of the maturing endosome. To test if the DOX cargo released into HeLa cells is functional, microscopy images (Fig. S4 in Appendix A) were recorded at 8 h post-delivery. Here, the test group exposed to acoustic waves (Fig. S4(b)) has more apoptotic cells and fewer cells attached to the Petri dish, compared to the control group that were not exposed to acoustic waves (Fig. S4(a)). The viability of HeLa cells significantly decreases over time (e.g., decreases to 73% after 2 h, 55% after 8 h, and 42% after 24 h), further confirming that the release of the cytotoxic chemothereutic agent reduces viability of the treated populations (Fig. S4(c)). To assess the efficiency of our acoustofluidic device quantitatively, we studied the delivery of DOX@ZIF-8 nanoparticles to HeLa cells and further characterized the delivery efficiencies through flow cytometry (Section 2 for procedures). From the results in Figs. 5(e) and (f), we find that the delivery efficiencies for cases without and with acoustic waves are ~18% and ~91%, respectively. The results also show that the measured mean fluorescence intensity increases from 2×10^2 (acoustics off) to 5×10^2 (acoustics on), indicating more DOX@ZIF-8 nanoparticles were delivered to the cells.

Through the above studies presented in this subsection, we have investigated and characterized different aspects of the intracellular delivery performance of our acoustofluidic approach. Our results demonstrate that ZIF-8 nanoparticles loaded with small molecules and proteins can be successfully delivered into acoustofluidically manipulated cells. The feasibility of our approach for suspension and adherent cells (such as U937 and HeLa cells) has been validated, and cell viability measurements (Fig. 4(e)) confirm that the acoustic waves and ZIF-8 decomposition minimally impact cell viability. Data from our flow cytometry studies (Figs. 5(e) and (f)) indicate that the delivery efficiency can be enhanced by introducing acoustic waves. We also investigated the mechanism of delivering cargo-encapsulated ZIF-8 nanoparticles and the release of functional cargos. The results (Figs. 5(a)–(d)) indicate that our acoustofluidic device enables controllable contact between flowed cells and nanoparticles coated on the wall of the device's microcapillary, facilitating cell-nanoparticle attachment.

4. Conclusions and Prospects

This study presents an effective acoustofluidics-based intracellular nanoparticle delivery platform that eliminates the need for bubbles or other specialized acoustic contrast agents typically required by conventional sonoporation methods [71]. Specifically, our approach leverages standing acoustic waves generated in a glass capillary to direct flowing cells to the capillary wall, which is coated with cargo–encapsulated ZIF-8 nanoparticles, thereby promoting membrane-nanoparticle attachment. Our experimental results revealed that cells were pushed against the capillary wall, slightly deformed, and transported along the wall,

indicating that cells were subjected to acoustic radiation forces and shear forces. Because of these forces, the cell membrane stress increases, potentially altering the membrane permeability. Additionally, our results show that the ZIF-8 nanoparticles are capable of encapsulating small molecules and protein-based cargos while enabling the controlled release of these cargos upon intracellular uptake. The combination of the above mechanisms enables our approach to achieve effective intracellular delivery.

Applying our acoustofluidic approach, we have performed a series of experiments to deliver ZIF-8 nanoparticles loaded with different cargos (DOX or FBSA) to two immortalized cancer cell lines (e.g., U937 cells and HeLa cells). The intracellular delivery of our nanoparticles (Figs. 5(e) and (f)) suggests that acoustic waves can significantly enhance the delivery efficiency of nanomaterials by inducing cell membrane distortion and constant membrane-nanoparticle contact. Furthermore, our results (Figs. 4(a) to (d)) confirm that two types of cargos (DOX and FBSA) can be successfully delivered to the cells, demonstrating the potential applications of our approach for delivering small molecules and protein-based cargos to cells beyond Brownian motion within microfluidic systems. Through investigation, characterization, and validation, this study has established an acoustofluidics-based intracellular delivery method that does not rely on microbubbles and advances state-of-the-art sonoporation technologies [72]. In the future, we will investigate the feasibility of our approach for delivering other types of cargo, such as nucleic acids and CRISPR/Cas9-based gene-editing constructs, and other carriers. We will test our approach using difficult-to-transfect primary human cell types (e.g., hematopoietic stem and progenitor cells and T cells) and investigate the feasibility of using the treated cells for *in vivo* studies. We anticipate that our acoustofluidics-based intracellular delivery platform can be applied for rapid manufacturing of engineered cell products for gene/cellular therapies as well as fundamental biophysical studies of cell mechanics in a controllable, scalable, and biocompatible manner.

Supplementary Material

Refer to Web version on PubMed Central for supplementary material.

Acknowledgments

We acknowledge the support from the National Institutes of Health (R01GM141055), the National Science Foundation (CMMI-2104295), the China Scholarship Council, and the NIH/NCATS UCLA CTSI (UL1TR001881) through the UC Center for Accelerated Innovation. This material is based upon work supported by the National Science Foundation Graduate Research Fellowship (1644868). Paul S. Weiss and Steven J. Jonas acknowledge support from the UCLA Innovation Fund MedTech Innovator Award and the Challenge Initiative at UCLA, and seed funding provided through a UCLA David Geffen School of Medicine Regenerative Medicine Theme Award. Steven J. Jonas acknowledges the support provided by the NIH Common Fund through an NIH Director's Early Independence Award co-funded by the National Institute of Dental and Craniofacial Research and Office of the Director, NIH under award number (DP5OD028181). Jason N. Belling thanks the NIH for a predoctoral fellowship supported by the National Heart, Lung, and Blood Institute of the National Institutes of Health under Award Number (F31HL149356).

Appendix A. Supplementary data

Supplementary data to this article can be found online at https://doi.org/10.1016/j.eng.2024.11.030.

References

[1]. Pelaz B, Alexiou C, Alvarez-Puebla RA, Alves F, Andrews AM, Ashraf S, et al. Diverse applications of nanomedicine. ACS Nano 2017;11(3):2313–81. [PubMed: 28290206]

[2]. Stewart MP, Langer R, Jensen KF. Intracellular delivery by membrane disruption: mechanisms, strategies, and concepts. Chem Rev 2018;118(16):7409–531. [PubMed: 30052023]

[3]. Chung YH, Cai H, Steinmetz NF. Viral nanoparticles for drug delivery, imaging, immunotherapy, and theranostic applications. Adv Drug Deliv Rev 2020;156:214–35. [PubMed: 32603813]

[4]. Yin H, Kanasty RL, Eltoukhy AA, Vegas AJ, Dorkin JR, Anderson DG. Non-viral vectors for gene-based therapy. Nat Rev Genet 2014;15(8):541–55. [PubMed: 25022906]

[5]. van Wamel A, Kooiman K, Harteveld M, Emmer M, ten Cate FJ, Versluis M, et al. Vibrating microbubbles poking individual cells: drug transfer into cells via sonoporation. J Control Release 2006;112(2):149–55. [PubMed: 16556469]

[6]. Yarmush ML, Golberg A, Serša G, Kotnik T, Miklavčič D. Electroporation-based technologies for medicine: principles, applications, and challenges. Annu Rev Biomed Eng 2014;16:295–320. [PubMed: 24905876]

[7]. Wang S, Wang H, Jiao J, Chen KJ, Owens GE, Kamei K, et al. Three-dimensional nanostructured substrates toward efficient capture of circulating tumor cells. Angew Chem Int Ed 2009;48(47):8970–3.

[8]. Wurm M, Zeng AP. Mechanical disruption of mammalian cells in a microfluidic system and its numerical analysis based on computational fluid dynamics. Lab Chip 2012;12(6):1071–7. [PubMed: 22311121]

[9]. Frost IM, Mendoza AM, Chiou TT, Kim P, Aizenberg J, Kohn DB, et al. Fluorinated silane-modified filtroporation devices enable gene knockout in human hematopoietic stem and progenitor cells. ACS Appl Mater Interfaces 2023;15(35):41299–309. [PubMed: 37616579]

[10]. Man T, Zhu X, Chow YT, Dawson ER, Wen X, Patananan AN, et al. Intracellular photothermal delivery for suspension cells using sharp nanoscale tips in microwells. ACS Nano 2019;13(9):10835–44. [PubMed: 31487464]

[11]. Stevenson DJ, Gunn-Moore FJ, Campbell P, Dholakia K. Single cell optical transfection. J R Soc Interface 2010;7(47):863–71. [PubMed: 20064901]

[12]. Koike S, Jahn R. Probing and manipulating intracellular membrane traffic by microinjection of artificial vesicles. Proc Natl Acad Sci USA 2017;114(46):E9883–92. [PubMed: 29087339]

[13]. Gao J, Bergmann T, Zhang W, Schiwon M, Ehrke-Schulz E, Ehrhardt A. Viral vector-based delivery of CRISPR/Cas9 and donor DNA for homology-directed repair in an *in vitro* model for canine hemophilia B. Mol Ther Nucleic Acids 2019;14:364–76. [PubMed: 30690229]

[14]. Pereyra AS, Mykhaylyk O, Lockhart EF, Taylor JR, Delbono O, Goya RG, et al. Magnetofection enhances adenoviral vector-based gene delivery in skeletal muscle cells. J Nanomed Nanotechnol 2016;7(2):364. [PubMed: 27274908]

[15]. Gresch O, Engel FB, Nesic D, Tran TT, England HM, Hickman ES, et al. New non-viral method for gene transfer into primary cells. Methods 2004;33(2):151–63. [PubMed: 15121170]

[16]. Cui J, Yan Y, Wang Y, Caruso F. Templated assembly of pH-labile polymer-drug particles for intracellular drug delivery. Adv Funct Mater 2012;22(22):4718–23.

[17]. Wan ACA, Ying JY. Nanomaterials for *in situ* cell delivery and tissue regeneration. Adv Drug Deliv Rev 2010;62(7–8):731–40. [PubMed: 20156499]

[18]. Zaman NT, Yang YY, Ying JY. Stimuli-responsive polymers for the targeted delivery of paclitaxel to hepatocytes. Nano Today 2010;5(1):9–14.

[19]. Broaders KE, Grandhe S, Fréchet JM. A biocompatible oxidation-triggered carrier polymer with potential in therapeutics. J Am Chem Soc 2011;133(4):756–8. [PubMed: 21171594]

[20]. Cai W, Chu CC, Liu G, Wang YX. Metal-organic framework-based nanomedicine platforms for drug delivery and molecular imaging. Small 2015;11(37):4806–22. [PubMed: 26193176]

[21]. Pegtel DM, Cosmopoulos K, Thorley-Lawson DA, van Eijndhoven MA, Hopmans ES, Lindenberg JL, et al. Functional delivery of viral miRNAs via exosomes. Proc Natl Acad Sci USA 2010;107(14):6328–33. [PubMed: 20304794]

[22]. Wang Z, Rich J, Hao N, Gu Y, Chen C, Yang S, et al. Acoustofluidics for simultaneous nanoparticle-based drug loading and exosome encapsulation. Microsyst Nanoeng 2022;8:45. [PubMed: 35498337]

[23]. Stewart MP, Sharei A, Ding X, Sahay G, Langer R, Jensen KF. *In vitro* and *ex vivo* strategies for intracellular delivery. Nature 2016;538(7624):183–92. [PubMed: 27734871]

[24]. Lu Y, Sun W, Gu Z. Stimuli-responsive nanomaterials for therapeutic protein delivery. J Controll Release 2014;194:1–19.

[25]. Doane TL, Burda C. The unique role of nanoparticles in nanomedicine: imaging, drug delivery and therapy. Chem Soc Rev 2012;41(7):2885–911. [PubMed: 22286540]

[26]. Hassan S, Prakash G, Bal Ozturk A, Saghazadeh S, Sohail MF, Seo J, et al. Evolution and clinical translation of drug delivery nanomaterials. Nano Today 2017;15:91–106. [PubMed: 29225665]

[27]. Li J, Cai C, Li J, Li J, Li J, Sun T, et al. Chitosan-based nanomaterials for drug delivery. Molecules 2018;23(10):2661. [PubMed: 30332830]

[28]. Buschmann MD, Carrasco MJ, Alishetty S, Paige M, Alameh MG, Weissman D. Nanomaterial delivery systems for mRNA vaccines. Vaccines 2021;9(1):65. [PubMed: 33478109]

[29]. Mahto SK, Yoon TH, Rhee SW. A new perspective on *in vitro* assessment method for evaluating quantum dot toxicity by using microfluidics technology. Biomicrofluidics 2010;4(3):034111. [PubMed: 20957065]

[30]. Deng Y, Kizer M, Rada M, Sage J, Wang X, Cheon DJ, et al. Intracellular delivery of nanomaterials via an inertial microfluidic cell hydroporator. Nano Lett 2018;18(4):2705–10. [PubMed: 29569926]

[31]. Hapala I Breaking the barrier: methods for reversible permeabilization of cellular membranes. Crit Rev Biotechnol 1997;17(2):105–22. [PubMed: 9192473]

[32]. Mcneil PL. Incorporation of macromolecules into living cells. Methods Cell Biol 1988;29:153–73.

[33]. Mead BP, Curley CT, Kim N, Negron K, Garrison WJ, Song J, et al. Focused ultrasound preconditioning for augmented nanoparticle penetration and efficacy in the central nervous system. Small 2019;15(49):1903460.

[34]. Kinoshita M, Hynynen K. Key factors that affect sonoporation efficiency in *in vitro* settings: the importance of standing wave in sonoporation. Biochem Biophys Res Commun 2007;359(4):860–5. [PubMed: 17568561]

[35]. Zhang P, Rufo J, Chen C, Xia J, Tian Z, Zhang L, et al. Acoustoelectronic nanotweezers enable dynamic and large-scale control of nanomaterials. Nat Commun 2021;12(1):3844. [PubMed: 34158489]

[36]. Tian Z, Shen C, Li J, Reit E, Bachman H, Socolar JES, et al. Dispersion tuning and route reconfiguration of acoustic waves in valley topological phononic crystals. Nat Commun 2020;11(1):762. [PubMed: 32034148]

[37]. Bruus H, Dual J, Hawkes J, Hill M, Laurell T, Nilsson J, et al. Forthcoming lab on a chip tutorial series on acoustofluidics: acoustofluidics—exploiting ultrasonic standing wave forces and acoustic streaming in microfluidic systems for cell and particle manipulation. Lab Chip 2011;11(21):3579–80. [PubMed: 21952310]

[38]. Friend J, Yeo LY. Microscale acoustofluidics: microfluidics driven via acoustics and ultrasonics. Rev Mod Phys 2011;83(2):647–704.

[39]. Reboud J, Bourquin Y, Wilson R, Pall GS, Jiwaji M, Pitt AR, et al. Shaping acoustic fields as a toolset for microfluidic manipulations in diagnostic technologies. Proc Natl Acad Sci USA 2012;109(38):15162–7. [PubMed: 22949692]

[40]. Collins DJ, Morahan B, Garcia-Bustos J, Doerig C, Plebanski M, Neild A. Two-dimensional single-cell patterning with one cell per well driven by surface acoustic waves. Nat Commun 2015;6:8686. [PubMed: 26522429]

[41]. Athanassiadis AG, Ma Z, Moreno-Gomez N, Melde K, Choi E, Goyal R, et al. Ultrasound-responsive systems as components for smart materials. Chem Rev 2022;122(5):5165–208. [PubMed: 34767350]

[42]. Fan Y, Zhang J, Wei B, Drinkwater BW. Controllable patterns and streaming of plane acoustic vortex with annular piezoelectric arrays excitation. Phys Fluids 2021;33(3):032009.

[43]. Aghaamoo M, Chen YH, Li X, Garg N, Jiang R, Yun JTH, et al. High-throughput and dosage-controlled intracellular delivery of large cargos by an acoustic–electric micro-vortices platform. Adv Sci 2022;9(1):2102021.

[44]. Naquin TD, Canning AJ, Gu Y, Chen J, Naquin CM, Xia J, et al. Acoustic separation and concentration of exosomes for nucleotide detection: ASCENDx. Sci Adv 2024;10(10):eadm8597. [PubMed: 38457504]

[45]. Yang S, Rufo J, Zhong R, Rich J, Wang Z, Lee LP, et al. Acoustic tweezers for high-throughput single-cell analysis. Nat Protoc 2023;18(8):2441–58. [PubMed: 37468650]

[46]. Yang S, Tian Z, Wang Z, Rufo J, Li P, Mai J, et al. Harmonic acoustics for dynamic and selective particle manipulation. Nat Mater 2022;21(5):540–6. [PubMed: 35332292]

[47]. Rufo J, Zhang P, Zhong R, Lee LP, Huang TJ. A sound approach to advancing healthcare systems: the future of biomedical acoustics. Nat Commun 2022;13(1):3459. [PubMed: 35710904]

[48]. Rufo J, Cai F, Friend J, Wiklund M, Huang TJ. Acoustofluidics for biomedical applications. Nat Rev Method Prim 2022;2(1):30.

[49]. Gu Y, Chen C, Mao Z, Bachman H, Becker R, Rufo J, et al. Acoustofluidic centrifuge for nanoparticle enrichment and separation. Sci Adv 2021;7(1):eabc0467. [PubMed: 33523836]

[50]. Zhang P, Bachman H, Ozcelik A, Huang TJ. Acoustic microfluidics. Annu Rev Anal Chem 2020;13(1):17–43.

[51]. Rich J, Tian Z, Huang TJ. Sonoporation: past, present, and future. Adv Mater Technol 2022;7(1):2100885. [PubMed: 35399914]

[52]. Ramesan S, Rezk AR, Dekiwadia C, Cortez-Jugo C, Yeo LY. Acoustically-mediated intracellular delivery. Nanoscale 2018;10(27):13165–78. [PubMed: 29964280]

[53]. Li X, Sun W, Fu W, Lv H, Zu X, Guo Y, et al. Advances in sensing mechanisms and micro/nanostructured sensing layers for surface acoustic wave-based gas sensors. J Mater Chem A 2023;11(17):9216–38.

[54]. Gong Z, Baudoin M. Three-dimensional trapping and dynamic axial manipulation with frequency-tuned spiraling acoustical tweezers: a theoretical study. Phys Rev Appl 2021;16(2):024034.

[55]. Zhang Z, Wang Y, Zhang H, Tang Z, Liu W, Lu Y, et al. Hypersonic poration: a new versatile cell poration method to enhance cellular uptake using a piezoelectric nano-electromechanical device. Small 2017;13(18):1602962.

[56]. Belling JN, Heidenreich LK, Tian Z, Mendoza AM, Chiou TT, Gong Y, et al. Acoustofluidic sonoporation for gene delivery to human hematopoietic stem and progenitor cells. Proc Natl Acad Sci USA 2020;117(20):10976–82. [PubMed: 32358194]

[57]. Sharei A, Zoldan J, Adamo A, Sim WY, Cho N, Jackson E, et al. A vector-free microfluidic platform for intracellular delivery. Proc Natl Acad Sci USA 2013;110(6):2082–7. [PubMed: 23341631]

[58]. Kang G, Carlson DW, Kang TH, Lee S, Haward SJ, Choi I, et al. Intracellular nanomaterial delivery via spiral hydroporation. ACS Nano 2020;14(3):3048–58. [PubMed: 32069037]

[59]. Zhang Y, Yu J, Bomba HN, Zhu Y, Gu Z. Mechanical force-triggered drug delivery. Chem Rev 2016;116(19):12536–63. [PubMed: 27680291]

[60]. Fu YQ, Luo JK, Nguyen NT, Walton AJ, Flewitt AJ, Zu XT, et al. Advances in piezoelectric thin films for acoustic biosensors, acoustofluidics and lab-on-chip applications. Prog Mater Sci 2017;89:31–91.

[61]. Zheng H, Zhang Y, Liu L, Wan W, Guo P, Nyström AM, et al. One-pot synthesis of metal-organic frameworks with encapsulated target molecules and their applications for controlled drug delivery. J Am Chem Soc 2016;138(3):962–8. [PubMed: 26710234]

[62]. Liang K, Ricco R, Doherty CM, Styles MJ, Bell S, Kirby N, et al. Biomimetic mineralization of metal-organic frameworks as protective coatings for biomacromolecules. Nat Commun 2015;6:7240. [PubMed: 26041070]

[63]. Alsaiari SK, Patil S, Alyami M, Alamoudi KO, Aleisa FA, Merzaban JS, et al. Endosomal escape and delivery of CRISPR/Cas9 genome editing machinery enabled by nanoscale zeolitic imidazolate framework. J Am Chem Soc 2018;140(1):143–6. [PubMed: 29272114]

[64]. Garofalo F, Laurell T, Bruus H. Performance study of acoustophoretic microfluidic silicon-glass devices by characterization of material- and geometry-dependent frequency spectra. Phys Rev Appl 2017;7(5):054026.

[65]. Chen WH, Luo GF, Vázquez-González M, Cazelles R, Sohn YS, Nechushtai R, et al. Glucose-responsive metal-organic-framework nanoparticles act as “smart” sense-and-treat carriers. ACS Nano 2018;12(8):7538–45. [PubMed: 29969227]

[66]. Liang Z, Yang Z, Yuan H, Wang C, Qi J, Liu K, et al. A protein@metal-organic framework nanocomposite for pH-triggered anticancer drug delivery. Dalton Trans 2018;47(30):10223–8. [PubMed: 30014058]

[67]. Chen TT, Yi JT, Zhao YY, Chu X. Biomineralized metal-organic framework nanoparticles enable intracellular delivery and endo-lysosomal release of native active proteins. J Am Chem Soc 2018;140(31):9912–20. [PubMed: 30008215]

[68]. Ren H, Zhang L, An J, Wang T, Li L, Si X, et al. Polyacrylic acid@zeolitic imidazolate framework-8 nanoparticles with ultrahigh drug loading capability for pH-sensitive drug release. Chem Commun 2014;50(8):1000–2.

[69]. Hur J, Park I, Lim KM, Doh J, Cho SG, Chung AJ. Microfluidic cell stretching for highly effective gene delivery into hard-to-transfect primary cells. ACS Nano 2020;14(11):15094–106. [PubMed: 33034446]

[70]. Yaghoubi A, Ramazani A. Anticancer DOX delivery system based on CNTs: functionalization, targeting and novel technologies. J Control Release 2020;327:198–224. [PubMed: 32763433]

[71]. Miller DL, Quddus J. Sonoporation of monolayer cells by diagnostic ultrasound activation of contrast-agent gas bodies. Ultrasound Med Biol 2000;26(4):661–7. [PubMed: 10856630]

[72]. Carugo D, Ankrett DN, Glynne-Jones P, Capretto L, Boltryk RJ, Zhang X, et al. Contrast agent-free sonoporation: the use of an ultrasonic standing wave microfluidic system for the delivery of pharmaceutical agents. Biomicrofluidics 2011;5(4):044108.

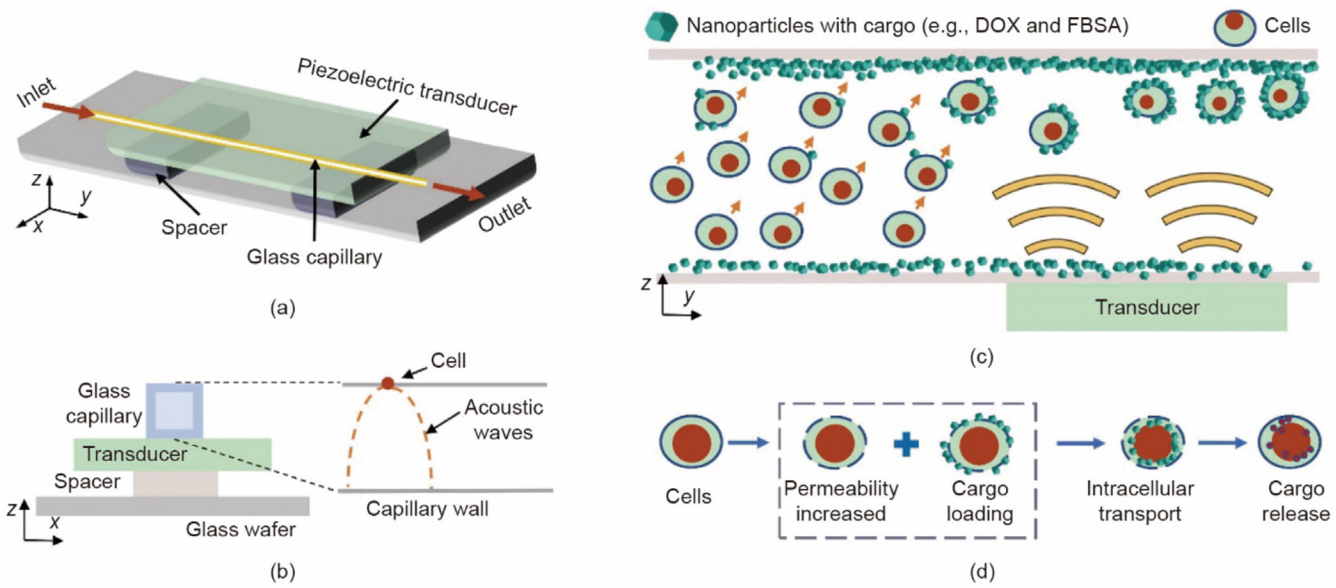

Fig. 1.

Schematics illustrating the mechanism of our acoustofluidics-based intracellular delivery device. (a) Device schematic. (b) Cross-sectional view of the device for illustrating the generation of standing bulk acoustic waves with a pressure node at the top capillary wall, which can push a cell loaded in the capillary to the top wall. (c) Illustration of the cell movement in a capillary coated with cargo-encapsulated nanoparticles under continuous flow and acoustic waves. The acoustic waves can push cells to the top wall, enabling controllable contact between cells and nanoparticles when the cells flow through the capillary along its top wall. (d) A schematic illustrating the intracellular cargo delivery process.

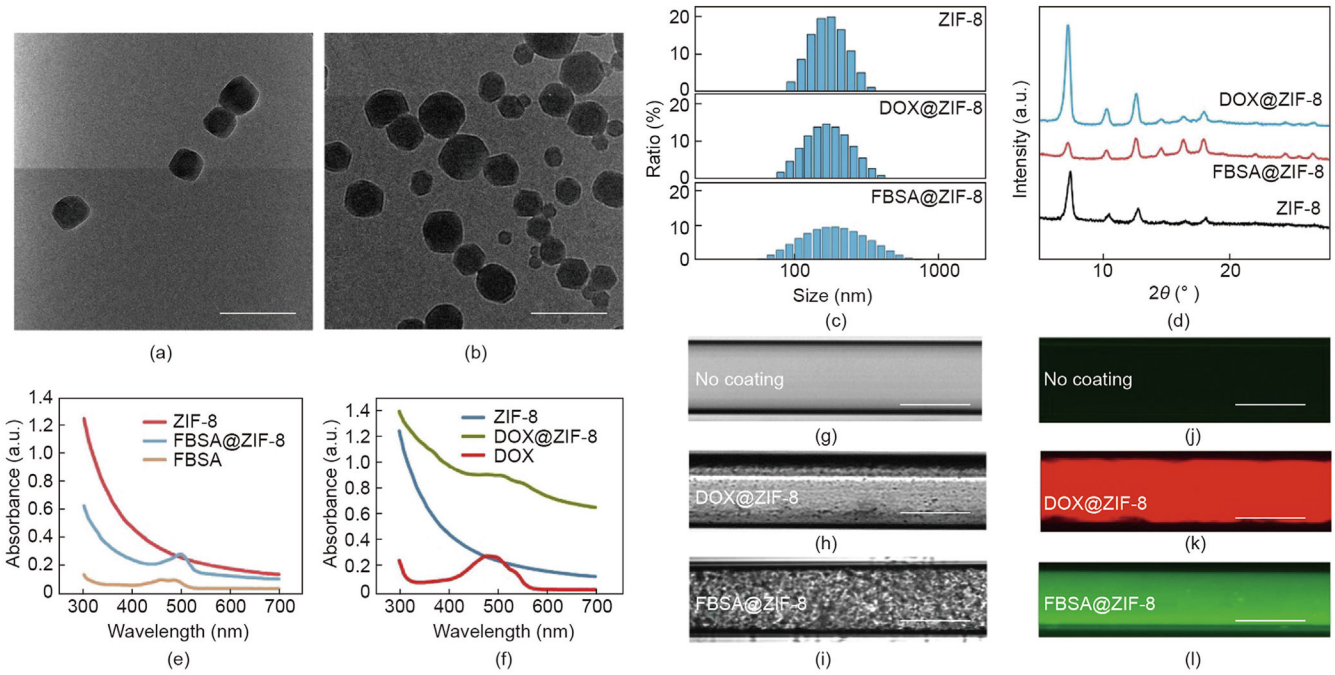

Fig. 2.

Characterization of cargo-encapsulated nanoparticles and nanoparticle-coated capillary walls. (a, b) TEM images of FBSA@ZIF-8 and DOX@ZIF-8 nanoparticles (scale bars: 250 nm). (c) DLS particle size distributions and (d) PXRD results for ZIF-8, DOX@ZIF-8, and FBSA@ZIF-8 nanoparticles. (e, f) UV-Vis absorbance spectrum distributions for FBSA@ZIF-8 and DOX@ZIF-8 nanoparticles. Bright-field and fluorescence images for (g, j) an original glass capillary wall without coating, (h, k) a DOX@ZIF-8 coated glass capillary wall, and (i, l) an FBSA@ZIF-8 coated glass capillary wall (scale bars: 150 μm). 2θ: the diffraction angle.

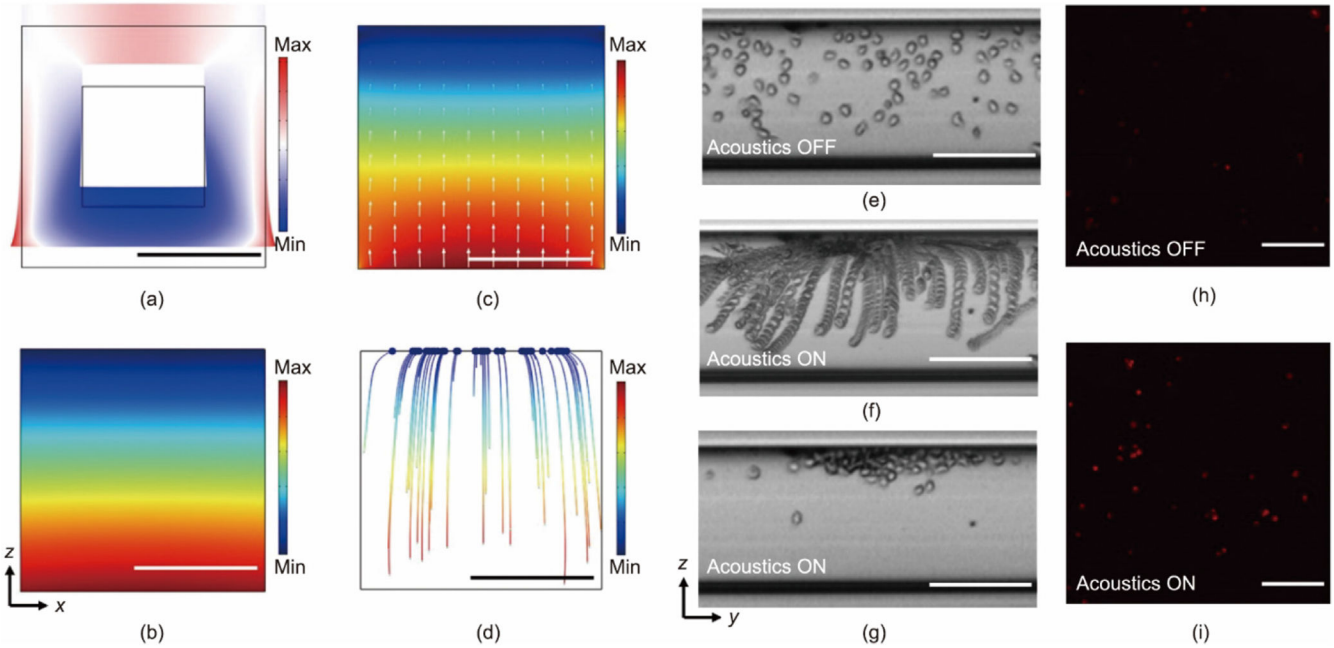

Fig. 3.

Acoustic wave-induced cell movement and permeability changes. (a) Finite element simulation result showing the displacement field of a glass capillary at the acoustic excitation frequency of 710 kHz. (b–d) Simulation results for the acoustic pressure field, the acoustic radiation force field, and the cell movement trajectories in the fluid domain, respectively. Max: maximum; Min: minimum. (e) Microscopy image for showing randomly distributed U937 cells in a capillary without acoustic waves. (f) Stacked microscopy images illustrating the trajectories of acoustic wave-induced cell movements. (g) Microscopy image demonstrating that cells can be pushed to the top capillary wall within 4 s by the acoustic waves. (h, i) Fluorescence microscopy images of U937 cells treated without and with acoustic waves. The cells were mixed with DOX@ZIF-8 nanoparticles in a solution and then loaded into clean capillaries without nanoparticle coating. The treated cells were collected from the capillaries, washed with PBS, and then dispensed on microscope slides for imaging. Scale bars: 100 μm.

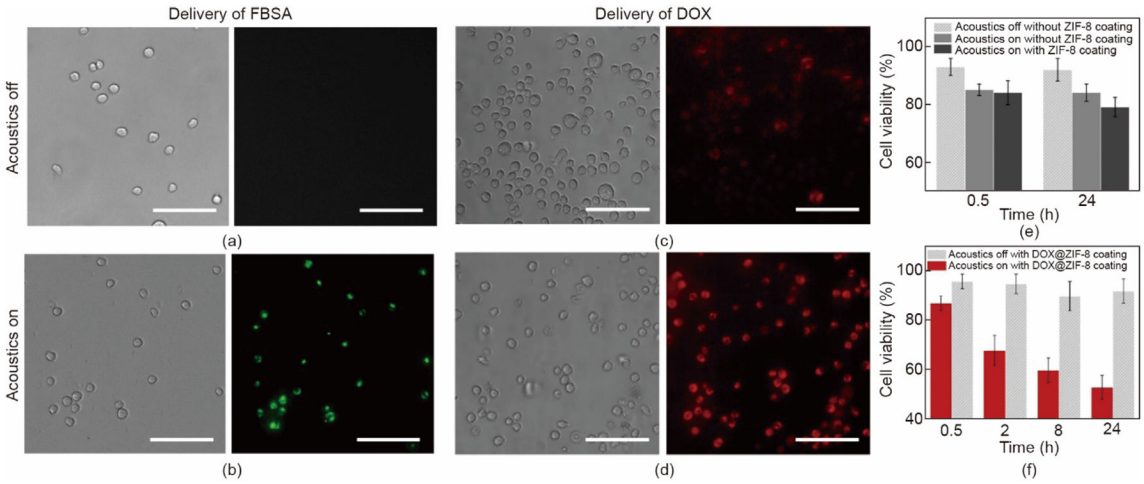

Fig. 4.

Testing delivery of different types of cargo. (a, b) Microscopy images (left: bright-field, right: fluorescence) showing the delivery of FBSA into U937 cells with acoustic waves off and on, respectively (scale bars: 100 μm). In these experiments, the glass capillaries were coated with FBSA@ZIF-8 nanoparticles. (c, d) Microscopy images (left: bright-field, right: fluorescence) showing the delivery of DOX into U937 cells with acoustic waves off and on, respectively (scale bars: 100 μm). In these experiments, the glass capillaries were coated with DOX@ZIF-8 nanoparticles. (e) Results of viability studies for three different cases. This data indicate that the used acoustic waves and nanocarriers have low cytotoxicities. (f) Results of viability studies for delivering DOX@ZIF-8 nanoparticles with and without acoustic waves. In the case of active acoustic waves, the cell viability gradually decreases over time because the successfully delivered DOX@ZIF-8 nanoparticles gradually release cytotoxic DOX, which induces cell apoptosis. The column heights and error bars in (e, f) represent the mean values and standard deviations, respectively.

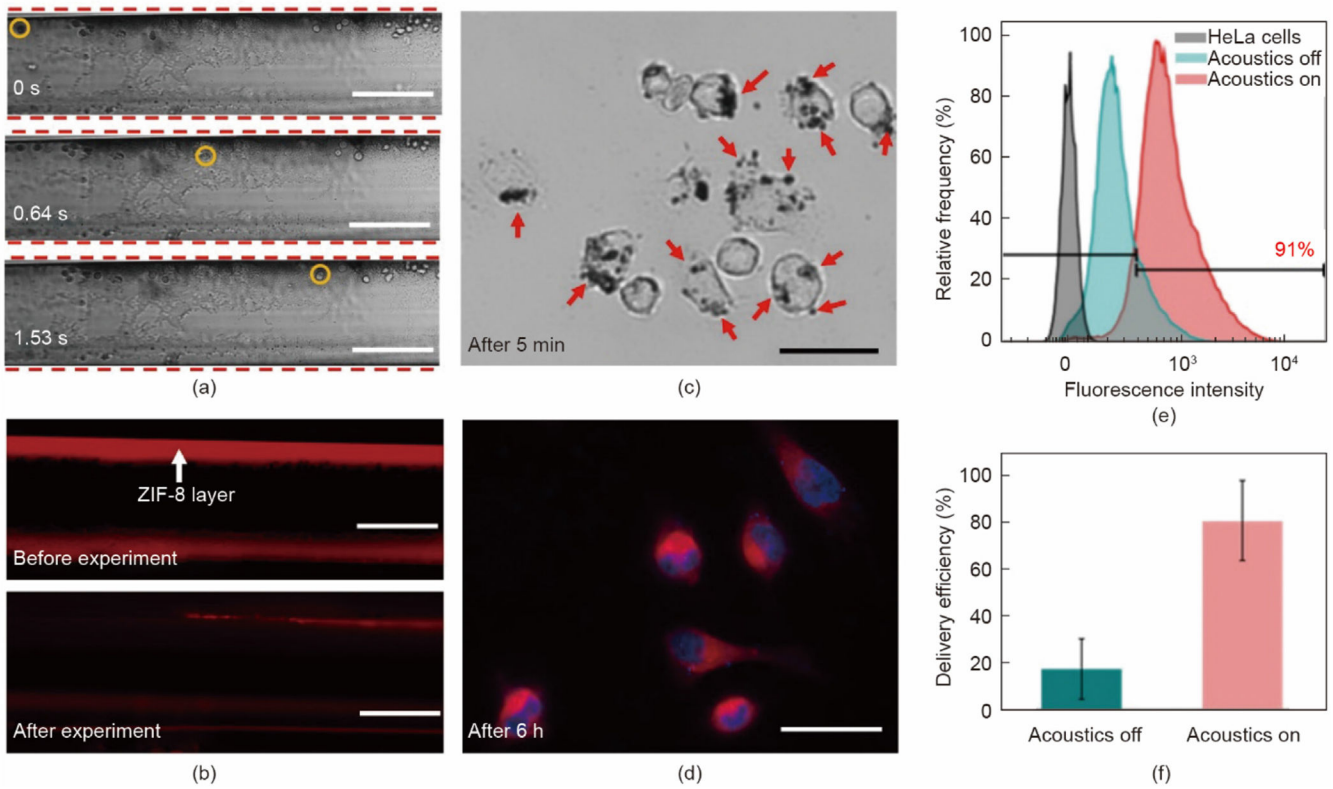

Fig. 5.

Acoustofluidic delivery of cargo-encapsulated nanoparticles into HeLa cells. (a) Time-lapse microscopic images for showing the movement of a cell (in yellow circles) along a capillary wall coated with DOX@ZIF-8 nanoparticles (scale bars: 100 μm). (b) Fluorescent images of a coated capillary before and after an intracellular delivery experiment (scale bar: 100 μm). (c) Bright-field microscopy image acquired 5 min after the experiment showing HeLa cells with attached DOX@ZIF-8 nanoparticles marked with red arrows (scale bar: 20 μm). (d) Fluorescence microscopy image acquired 6 h after the experiment showing DOX molecules in cells (scale bar: 20 μm, red: DOX, blue: DAPI for nucleus). These DOX molecules, which are released from the successfully delivered DOX@ZIF-8 nanoparticles, gradually cause cell apoptosis, as confirmed by the cell morphology changes and the viability decreases shown in Fig. S4. (e, f) Flow cytometry results for delivering DOX@ZIF-8 nanoparticles into HeLa cells ($N = 3$).